Robust detection of tandem repeat expansions from long DNA reads

Satomi Mitsuhashi [1,*†], Martin C Frith [2-4,*†], Takeshi Mizuguchi [1], Satoko Miyatake[1], Tomoko Toyota [5], Hiroaki Adachi [5], Yoko Oma [6], Yoshihiro Kino [7], Hiroaki Mitsuhashi [8], Naomichi Matsumoto [1]

1. Department of Human Genetics, Yokohama City University Graduate School of Medicine

2. Artificial Intelligence Research Center, National Institute of Advanced Industrial Science and Technology (AIST)

3. Graduate School of Frontier Sciences, University of Tokyo

4. Computational Bio Big-Data Open Innovation Laboratory (CBBD-OIL), AIST

5. Department of Neurology, University of Occupational and Environmental Health School of Medicine

6. Department of Liberal Arts, Faculty of Medicine, Saitama Medical University

7. Department of Bioinformatics and Molecular Neuropathology, Meiji Pharmaceutical University

8. Department of Applied Biochemistry, School of Engineering, Tokai University

[†] These authors are contributed equally

* Corresponding authors:

Martin C Frith, PhD

Artificial Intelligence Research Center

National Institute of Advanced Industrial Science and Technology (AIST)

2-3-26 Aomi, Koto-ku, Tokyo, 135-0064, Japan

Telephone: +81-3-3599-8001

Fax: +81-3-5530-2061

E-mail: mcfrith@edu.k.u-tokyo.ac.jp

Satomi Mitsuhashi, MD, PhD

Department of Human Genetics

Yokohama City University Graduate School of Medicine

Fukuura 3-9, Kanazawa-ku, Yokohama, 236-0004, Japan

Telephone: +81-45-787-2606

Fax: +81-45-786-5219

E-mail: satomits@yokohama-cu.ac.jp

Abstract

Tandemly repeated sequences are highly mutable and variable features of genomes. Tandem repeat expansions are responsible for a growing list of human diseases, even though it is hard to determine tandem repeat sequences with current DNA sequencing technology. Recent long-read technologies are promising, because the DNA reads are often longer than the repetitive regions, but are hampered by high error rates. Here, we report robust detection of human repeat expansions from careful alignments of long (PacBio and nanopore) reads to a reference genome. Our method (`tandem-genotypes`) is robust to systematic sequencing errors, inexact repeats with fuzzy boundaries, and low sequencing coverage. It is easily usable to find known-pathological or suspicious repeat expansions, which have tended to be overlooked in recent genetic studies. This may help to elucidate the many genetic diseases whose causes remain unknown.

Introduction

A tandem repeat is a region where multiple adjacent copies of sequence reside in the genomic DNA. These regions are highly variable among individuals due to replication error during cell division. They are a source of phenotypic variability in disease and health. More than 30 human diseases are caused by copy-number alterations in tandem repeats[1].

The range of pathogenic copy number change relative to the reference varies from a few to several thousand, and the length of repeating unit varies from e.g. three (triplet-repeat disease) to several thousand (macro-satellite repeat). As might be expected from such diverse underlying genetic causes, disease mechanisms are also variable. Well-known examples of triplet-repeat expansion diseases in protein-coding regions are polyglutamine diseases (e.g. spinal and bulbar muscular atrophy, Huntington's disease)[2,3]. Triplet-repeat expansion of CAG or CAA codons, which encode glutamine, leads to toxic protein aggregation and neuronal cell death. Another example of triplet-repeat disease is caused by CUG repeat expansion in the 3'UTR of the transcript from the *DMPK* gene, producing a toxic gain-of-function transcript which sequesters

splicing factor proteins and causes aberrant splicing, resulting in multiple symptoms[4]. Not only gain-of-function mutations, but also loss-of-function repeat change in the promoter region due to transcriptional silencing has been reported (e.g. fragile X syndrome)[5]. In addition to short tandem repeat diseases, repeat copy-number aberration in human disease is also reported in a macro-satellite repeat (D4Z4). Shortening of the D4Z4 repeat causes aberrant expression of the flanking gene *DUX4*, which has a toxic effect in muscle cells[6]. The thresholds of pathogenic repeat expansion in coding regions are usually less than 100 copies and sometimes even a few copy differences can cause disease (e.g. oculopharyngeal muscular dystrophy)[7]. In contrast, some disease causing tandem-repeat expansions in introns or UTRs can be very long (e.g. *DMPK*)[4]. Moreover, some repeats are interrupted by different sequences (e.g. *DMPK*, *ATXN10*, *SAMD12*)[8-10], making it difficult to analyze the precise repeat structure.

It has been roughly a decade since the introduction of high throughput short read sequencers to clinical genetics. There have been numerous successful identifications of small nucleotide changes, especially in coding

regions, mainly thanks to targeted sequencing (e.g. whole exome sequencing). However, the diagnostic rate remains 30% (depending on the diagnostic platform used)[11], leaving a large population of Mendelian diseases unsolved. There may be many reasons, but one of the simplest is that the remaining patients may have mutations in "non-coding regions", or they may have mutations in coding regions which were overlooked due to the limitations of short read sequencing. One candidate is tandem repeat regions, which are difficult to analyze genome-wide by conventional techniques. Identification of disease-causing tandem repeat changes is usually realized by classical genetic technologies (i.e. linkage analysis, Southern blot, etc.) and targeted repeat region analysis in a large number of families.

The recent advancement of long read sequencing technologies may provide a good solution, because long enough reads can encompass whole expanded repeats, and can be analyzed using the flanking unique sequences. Long read sequencers such as PacBio or nanopore sequencers have been coming to clinical genetics very recently. As of 2018, these technologies are

continually improving in terms of accuracy and data output. However, in the clinical laboratory, it is still difficult due to cost-efficiency and the computing burden for large data. It would be preferable, and realistic, if low coverage data (~10X) can be used to detect alteration of tandem repeats.

We are aware of two previous methods for determining tandem repeat copy number from long DNA reads: PacmonSTR and RepeatHMM[12-13]. These methods: align the reads to a reference genome, then get the reads that cover a tandem repeat region of the reference, and perform sophisticated probability-based comparisons of these reads to the sequence of the repeating unit. In this study, however, we find that these methods do not always succeed with current long-read data.

We have recently advocated a method (using the LAST software) for aligning DNA reads to a genome allowing for rearrangements and duplications[14]. This method has two key features. First: it determines the rates of insertion, deletion, and each kind of substitution in the data, and uses these rates to determine the most probable alignments[15]. Second: it finds the most-probable

division of each read into (one or more) parts together with the most probable alignment of each part. This method found diverse types of rearrangement, the most common of which was tandem multiplication (e.g. heptuplication), often of tandem-repeat regions[14].

Here, we detect tandem repeat copy number changes by aligning long DNA reads to a reference genome with `LAST`, and analyzing these alignments in a crude-but-effective way. We point out several practical difficulties with analyzing tandem repeat sequences, which motivate our crude analysis method. Our approach is capable of analyzing tandem-repeats genome-wide even with relatively low coverage sequencing data. We believe that this tool will be very useful for identifying disease-causing mutations in tandem repeat regions which have been overlooked by short read sequencing in human disease.

Methods

tandem-genotypes method

`tandem-genotypes` (https://github.com/mcfrith/tandem-genotypes) has two required inputs: annotations of tandem repeats in a reference genome, and alignments of DNA reads to the same genome.

The annotations supply a start and end coordinate for each repeat, and the length *u* of its repeating unit. The repeat length need not be an integer multiple of the unit length. We define two ad hoc distances: "far" $f = \max[100, u]$ and "near" $n = \max[60, u]$. (Actually, we truncate *f* at the edge of the sequence: where we speak of *f*, we really mean min[*f*, distance to the edge of the reference sequence].)

`last-split` finds a division of each DNA read into (one or more) parts, and an alignment of each part to the genome. It gives each alignment a "mismap probability", which is high if that part of the read aligns almost equally well to other loci[14]. We regard one read's alignments as ordered by their 5' to 3' positions in the read.

For each DNA read, `tandem-genotypes` performs these steps:

1. Discard alignments with mismap probability > 10^{-6}.

2. Discard alignments of mostly-lowercase sequence. This removes alignments that consist almost entirely of simple sequence (such as atatatatata), which are less reliable. Simple sequence is detected and lowercased by `lastdb` and `lastal`, using `tantan`[16]. An alignment is discarded if it lacks any segment with score >= `lastal`'s score threshold, when "gentle masking" is applied[17].
3. Join consecutive alignments that are colinear on the same strand of the same chromosome.
4. Find all alignments that overlap a given repeat.

If there is one such alignment:

- Require that it extends beyond both sides of the repeat by at least *f*, else give up (i.e. don't use this DNA read for this repeat).
- Extract all "gaps" from the alignment. Here, one "gap" may have *d* unaligned reference bases and *i* unaligned query bases, flanked by aligned bases. For each gap:
    - If it does not overlap the repeat and *i* <= *u*/2: ignore it.

- If it is wholly >= *f* away from the repeat: ignore it.
- If it is partly >= *f* away from the repeat: give up.
- If it is wholly > *n* away from the repeat: ignore it.
- Define *r* to be the number of unaligned reference bases in the gap that are in the repeat.
- Define the gap's net deletion size: $D = \min(d - i, r)$.
- Assume this gap contributes an integer (or zero) copy-number change. Find this contribution by rounding *D* to the nearest multiple of *u* (breaking ties by rounding towards zero).

If there is more than one such alignment:

- Require that they are consecutive in the read, and on the same strand.
- Define the "left" alignment to be the first one if the strand is "+", else the last one. Define the "right" alignment in the opposite way.
- Require that the left alignment extends leftwards of the repeat, and leftwards of the other alignments, by at least *f*. Require that the other alignments do not extend leftwards of the repeat by *f* or more.

- Likewise for the right alignment.
- Define the insertion size as: the number of query bases, minus the number of reference bases (which could be negative), between the end of the left alignment and the start of the right alignment.
- Find the nearest multiple of *u* to this insertion size (as above).

Prioritization of copy number changes

The repeats are ranked by a priority score. Each repeat has multiple predictions of copy-number change, one per DNA read. Discard the most extreme expansion and contraction, take the most extreme remaining change, and calculate:

$$100 * |\text{length change in bases}| / (\text{reference repeat length} + 30).$$

(The + 30 prevents excessive scores for short reference repeats.) This score is multiplied by an ad hoc value per gene annotation, currently: 50 for coding, 20

for UTR, 15 for promoter, 15 for exon of non-protein-coding RNA, and 5 for intron. This is multiplied by 2 for coding annotations where the repeating unit codes polyglutamine or polyalanine in any reading frame (out of 6).

Public and patient human genome data and alignment to reference genome

Human whole genome nanopore (rel3) and PacBio (SRR3197748) sequence data from the same individual (NA12878) were downloaded from (https://github.com/nanopore-wgs-consortium/NA12878) and from the SRA database, respectively[18]. Another 60X coverage human whole genome nanopore dataset from a different individual (NA19240) using PromethION was downloaded from https://www.ebi.ac.uk/ena/data/view/PRJEB26791.

Genomic DNA from a human patient with BAFME phenotype was sequenced by PacBio Sequel according to the manufacturer's protocol. Briefly, genomic DNA was sheared by g-TUBE (Covaris, MA, USA), then size selection was done by

BluePipin (Sage science, MA, USA) according to the standard method. These datasets were aligned to the human genome (GRCh38) with `LAST` version 936:

```
windowmasker -mk_counts -in genome.fa > genome.wmstat
windowmasker -ustat genome.wmstat -outfmt fasta -in genome.fa > genome-wm.fa
lastdb -P8 -uNEAR -R11 -c GRCh38 genome-wm.fa
last-train -P8 GRCh38 reads.fasta > train.out
lastal -P8 -p train.out GRCh38 reads.fasta | last-split > alns.maf
```

Generating tandem-repeat containing plasmids

Plasmids containing various numbers of CAG, GGGGCC and CAA used for this study were generated as described elsewhere[19-21] and are available upon request (Supplemental Table1). Sequence data of the plasmids were deposited in (DRA007012, Table2).

A plasmid with CCTG repeats was generated as follows. Briefly, exon 1 with flanking 225 bp of intron 1 and exon 2 with flanking 1051 bp of intron 1 (including

interrupted $CCTG_{12}$ repeats) of the human *CNBP* gene were amplified by PCR using human genome DNA (cat.# G304A, Promega, Wisconsin, USA), and then cloned into pBluescriptII-KS(-) using In-Fusion cloning kit (Clontech Takara, Shiga, Japan). The resulting construct was digested with SalI and XhoI, and then ligated with T4 DNA ligase to delete the SalI site in the multicloning site of the pBluescriptII-KS(-). A new SalI enzyme site was generated by site-directed mutagenesis after 13bp of the interrupted $CCTG_{12}$ repeats, to obtain a pBS-CNBP-SalI vector. Oligo DNAs containing $CCTG_{15}$ repeats and flanking sequence, 5'-TCGA$(CCTG)_{15}$C-3' and 5'-TCGAC$(CAGG)_{15}$-3', were phosphorylated by T4 polynucleotide kinase, annealed, and then ligated using T4 DNA ligase (Takara, Shiga, Japan). The resulting ligated oligo DNA was digested with SalI and XhoI to remove undesired DNA fragments. Three tandemly ligated oligos were cloned into the SalI site of the pBS-CNBP-SalI vector. This plasmid has $CCTG_{45}$ repeats interrupted by CTCGA in every 15 CCTG repeats, named interrupted $CCTG_{45}$ ($iCCTG_{45}$).

Nanopore sequencing and alignment of tandem-repeat containing plasmids

These repeat-containing plasmids were digested with restriction enzymes NheI, EcoRI-HF, BamHI-HF or DraIII (NEB, MA, USA) (Supplemental Table 1) and then treated with Klenow Fragment DNA Polymerase (Takara, Shiga, Japan) at 37°C for 30 min. The whole DNA fragments were purified using AmPureXT beads (Agilent Techinologies, CA, USA), then subjected to nanopore sequencing. Library preparation was performed using a 1D Native barcoding genomic DNA kit (EXP-NBD103 and SQK-LSK108) then subjected to MinION (Oxford Nanopore Techonologies) sequencing using one FLA-MIN106(R9.4.1) flowcell according the manufacturer's protocol. Base-calling and fastq conversion were performed with MinKNOW ver1.11.5. De-barcoding was done using EPIME software (Oxford Nanopore Techonologies).

Obtained fastq files were transformed to fasta files using `seqkit` fq2fa option (http://bioinf.shenwei.me/seqkit). fasta files were aligned to plasmid references like this;

```
lastdb -P8 -uNEAR -R01 plasmid-ref plasmid.fasta

last-train -P8 plasmid-ref reads.fasta > train.out

lastal -P8 -p train.out plasmid-ref reads.fasta | last-split > alns.maf
```

SCA10 data

SCA10 sequences from three patients with spinocerebellar ataxia 10 (MIM: 603516)[9] were downloaded from SRA (subjectA: SRR2080459, subjectB: SRR2081063, subjectC-1: SRR2082412, subjectC-2: SRR2082428) then fasta files were generated by this command;

```
fastq-dump --fasta --table SEQUENCE --split-spot --skip-technical -I --gzip
```

Reads were aligned to the human genome (GRCh38) like this;

```
lastdb -P8 -uNEAR -R01 GRCh38 reference.fasta

last-train -P8 GRCh38 reads.fasta > train.out

lastal -P8 -p train.out GRCh38 reads.fasta | last-split > alns.maf
```

Comparison to RepeatHMM and PacmonSTR

The SCA10 and BAFME reads were analyzed as follows.

PacmonSTR:

`blasr` fasta reference.fa -m 5 --out blasr.out.m5

`makeBinnedAnchors.py` blasr.out.m5 simpleRepeat.txt 100

`pacMonStr_V1.py` blasr.out.m5 binned_anchors 10 8 current_directory_path

RepeatHMM:

`repeatHMM.py` FASTQinput --fastq fastq --Patternfile hg38.predefined.pa

--repeatName gene --hgfile reference.fa

`repeatHMM.py` BAMinput --Onebamfile bam --Patternfile hg38.predefined.pa

--repeatName gene --hgfile reference.fa

For SCA10 subjectA and subjectC-2, after consulting the RepeatHMM authors,

we re-ran it with these options added: '--CompRep AlTIT50/C50lCIT/C

--SplitAndReAlign 1'.

Running tandem-genotypes

The copy number changes of tandem repeats were determined by t

`tandem-genotypes` with some different options.

To check all tandem repeats in the human genome in NA12878 data (rel3 and SRR3197748);

```
tandem-genotypes -u 1 -g refFlat.txt rmsk.txt alns.maf
```

To check disease-related tandem repeats in chimeric reads, BAFME and SCA10 data;

```
tandem-genotypes hg38-disease-tr.txt alns.maf
```

To check the plasmid sequences;

```
tandem-genotypes plasmid-repeat.bed alns.maf
```

Tandem repeat (rmsk.txt) and gene (refFlat.txt) annotations were obtained from the UCSC genome database (http://genome.ucsc.edu/)[22]. We made the file

hg38-disease-tr.txt, with 31 disease-associated tandem repeats, based on Tang *et al.*[1].

Chimeric reads of plasmid-derived repeats and human-derived flanks

Human nanopore reads covering repeat expansion disease loci were extracted from whole genome sequence data (rel3). The nanopore sequences flanking the repeat were excised using an in-house script. Randomly selected expanded and non-expanded repeat sequences were excised from plasmid nanopore sequences, using `maf-cut`. Then, these expanded and non-expanded repeats were inserted between the flanks, to generate chimeric reads. The combinations of repeat copy and number of rel3 reads are shown in Table 1, imitating the diploid genome. The chimeric reads were aligned to GRCh38 as mentioned above with `WindowMasker`[23].

Dot-plot pictures were made with last-dotplot using the following command;

`last-dotplot` --max-gap2=0,inf --rmsk1 rmsk.txt aln.maf file.png

PCR amplification of inexact repeats in rel3 and PacBio data

Two inexact tandem-repeats were tested by PCR and Sanger sequencing. Primers are described in Supplemental Table 2. PCR amplification was done using KAPA HiFi HS DNA polymerase (Kapa Biosystems, Basel, Switzerland). DNA for NA12878 was obtained from the Coriell Institute (https://coriell.org). PCR products were cloned into pCR-Blunt vector (Thermo Fisher Scientific, MA, USA) and subjected to Sanger sequencing.

Ethics

The Institutional Review Board of Yokohama City University of Medicine approved the experimental protocols. Informed consent was obtained from the patient, in accordance with Japanese regulatory requirements.

Results

Nanopore sequencing of tandem-repeat containing plasmids

We tested plasmids with four different kinds of repeat (CAG, CAA, GGGGCC and iCCTG) that are known to cause human diseases. The CAG plasmids have 5 different copy numbers (6, 18, 30, 70 and 130). The CAA and GGGGCC plasmids have two different copy numbers, 15/109 and 21/52, respectively. These plasmids were subjected to Oxford Nanopore Technologies' (ONT) MinION sequencing. The MinION reads were aligned to plasmid reference sequences with copy number 6 (CAG), 15 (CAA), 3 (GGGGCC), and 15 (CCTG). `tandem-genotypes` predicts the copy number change in each read: these predictions roughly agree with the actual copy number changes (Figure 1, red arrows). There is a minority of unexpectedly low copy number predictions (Fig1d,i; arrow), especially for the longer plasmids: manual inspection of alignment dotplots (not shown) suggests that these are correct, and the copy numbers in these plasmids may not be completely stable.

In one case, pBS-(CAG)30, `tandem-genotypes` fails with almost no predictions. pBS-(CAG)30 was digested at an enzyme site very near the repeat region (10-bp upstream), so there is only 10 bp of non-repeat sequence

upstream of the repeat, which is too short for step 2 of `tandem-genotypes`. Thus, we digested the same plasmid with a different enzyme, DraIII, far from the start of the repeat. As expected, the `tandem-genotypes` prediction agrees with the actual copy number change (Supplemental Figure 1a, red arrows).

The GGGGCC repeats have bimodal copy number predictions, where the two modes correspond to reads from each DNA strand (Fig 1h-i, Supplemental Fig 1b). This can be explained by sequence-specific sequencing error tendencies[24] that differ for the forward- and reverse-strand repeat sequences.

In human genomic sequencing, it might be difficult to obtain deep coverage such as 1000X as we have done for these plasmids, due to cost. For some repeat expansion diseases, such as polyglutamine disease, disease-causing copy number change thresholds from the controls are usually less than 100. To test the ability of `tandem-genotypes` to distinguish fine copy number differences of these plasmids even with low coverage, we randomly picked 50, 30 and 15 reads from each dataset and compared the copy number

predictions. Even with low coverage (15X) it is not difficult to distinguish copy numbers 18, 30, 70 and 130 for CAG repeats; 15 and 109 for CAA repeats; 21 and 52 for GGGGCC repeats (Figure 2).

Analyzing chimeric human/plasmid nanopore reads

We performed further tests on semi-artificial data. We obtained human nanopore reads that cover 10 disease-associated repeat regions, and replaced the repeat region in each read with the repeat region of a plasmid nanopore read. We used plasmid repeat regions with disease-causing and healthy repeat copy numbers in 1:1 ratio (Table1). These chimeric reads were aligned to a reference human genome, and copy-number changes were predicted. For each repeat, the predictions have clear bimodal distributions (Figure 3). As these plasmid-origin repeats were expected to vary because of nanopore base-call error or replication error in *Escherichia coli* during plasmid preparation, we also made chimeric sequences by inserting the exact number of exact repeats, to test the accuracy of `tandem-genotypes`. The results were improved in all cases

(Figure 3), in particular the *C9orf72* case with large strand-bias, indicating that deviations from the projected copy numbers are due to nanopore sequencing errors or replication error, and not systematic errors of `tandem-genotypes`.

Pacbio sequencing datasets of patients with SCA10

Next, we examined four PacBio sequencing datasets of cloned PCR amplification products from the SCA10 disease locus (spinocerebellar ataxia 10, MIM 603516). SCA10 is caused by ATTCT expansion in the intron of *ATXN10*. These datasets are from three unrelated patients: A, B and C[9]. Patient C has two datasets, C-1 and C-2, which are different clones sequenced with different PacBio chemistries. According to McFarland et al., subjects A, B and C can be estimated to have 4.5 kb, 3.9 kb and 2.7 kb repeat expansions (since PCR product sizes are 6.5 kb, 5.9 kb and 4.7 kb and they contain 2 kb flanking sequences), respectively[9]. `tandem-genotypes` predicted datasets A, B, C-1 and C-2 have average expansions of 913, 841, 484 and 486 copies relative to the reference (14 copies), hence repeat lengths 4.6 kb, 4.3 kb, 2.5 kb and 2.5 kb

respectively (Figure 4a). Thus subject B is predicted to have 0.4 kb larger repeat size than the PCR product, however from McFarland et al. Figure 1b[9], the purified clone they sequenced by PacBio had > 6 kb insertion, making the actual repeat size > 4 kb, closer to our prediction.

The same datasets were also analyzed with RepeatHMM and PacmonSTR. We first ran RepeatHMM with straightforward parameters: for subject A it found a similar peak to us but also an unexpected peak around zero, and it did not find the expected peaks for the other three datasets (Figure 4b). We then consulted the RepeatHMM authors, who suggested non-obvious parameters that improved the C-2 result, but there was still a peak around zero (Figure 4c). PacmonSTR did not detect the expected repeat numbers (data not shown).

PCR and Sanger sequencing of non-exact expanded repeats in NA12878

Repeat annotations (i.e. rmsk from UCSC) include non-exact tandem-repeats. Non-exact or interrupted tandem-repeats sometimes cause

human disease[8]. We detected inexact repeat expansions in the NA12878 human genome, by applying `tandem-genotypes` to the PacBio and MinION datasets.

In an intron of *PCDH15*, rmsk annotates a "TATAT" tandem repeat (chr10:54421448-54421530), though the actual sequence is not exactly TATAT (tatataaaataaactttattatatttagcatttgatttttatttatgtatattataaaatgaatatagtttatattataata). `tandem-genotypes` found two peaks for this repeat, indicating a heterozygous ~300 bp insertion (Figure 5a). PCR amplification of this region showed two different products possibly from different alleles. One had the same length as the reference sequence (PCDH15-intron-repeat-S) (Figure 5a). Sanger sequence of the other longer PCR product (PCDH15-intron-repeat-L) revealed a ~332 bp insertion. Surprisingly, this insertion was not a tandem expansion, but rather an AluYb8 SINE (according to RepeatMasker).

We also examined an intergenic GT tandem repeat (chr8:48173947-48174212). `tandem-genotypes` found one peak indicating an insertion of ~1000 bp (Figure 5b). PCR of this region showed single product from

this tandem repeat region, estimated to contain a ~1000 bp insertion. Sanger sequencing revealed that this expansion includes not only GT but also some unknown sequence. The expanded sequence is present in the chimpanzee genome (Figure 5b), indicating that this is actually a deletion in the human reference genome (which may have occurred by recombination between GT tandem repeats).

These two examples indicate that `tandem-genotypes` can also find complex and interrupted expansions (or non-deletions) of tandem repeats.

Pacbio sequencing of a patient with BAFME

We further analyzed PacBio whole genome sequencing of a patient with a phenotype of benign adult familial myoclonic epilepsy (BAFME). In another large number of BAFME patients in Japan[10], the cause was attributed to large expansions of intronic TTTCA and TTTTA repeats in *SAMD12*. We wished to know whether our patient has such an expansion in *SAMD12*. We sequenced this patient's genomic DNA using a PacBio Sequel sequencer.

`tandem-genotypes` detected ~5 kb insertion in three reads at the BAFME locus, where the coverage is 6X (Figure 6a). We also applied RepeatHMM and PacmonSTR to this dataset, but they failed to predict any expansions.

Some difficulties with tandem repeat analysis

The three expanded BAFME reads do not align to the repetitive region as would be expected for a straightforward repeat expansion (Figure 6b). Read 2, from the forward genome strand, does not align to the repetitive region at all, because its expanded region consists mostly of TCCCC repeats whereas the forward strand of the reference genome has TAAAA repeats (Supplemental Figure 2). Reads 1 and 6, from the reverse genome strand, align to the repeat at only one side of the expansion. The expanded regions of these two reads start with TTTTA repeats, which match the reverse strand of the reference, but mostly consist of TTTTC repeats. Since the expanded region of read 2 does not match the reverse complement of read 1 or 6, we infer that systematic sequencing error

has occurred on at least one strand. Short-period tandem repeats are prone to a nasty kind of sequencing error: if a systematic error occurs for one repeat unit, the same error will tend to occur for all the other units, producing a different repeat (which may align elsewhere in the genome: the main reason for step 2 in `tandem-genotypes`).

Another kind of difficulty is illustrated by our chimeric human/plasmid reads for *ATXN7* (Figure 6c). Here, the reference sequence adjacent to the annotated repeat is similar to the sequence within the repeat. Depending on the exact sequences and alignment parameters, the expanded region of a read may align outside the repeat annotation (Figure 6c top), or appear as alignment gaps some distance beyond the repeat (Figure 6c bottom). `tandem-genotypes` handles such cases, up to a point, by examining the alignments out to ad hoc distances beyond the annotated repeat.

Specificity of repeat-expansion predictions

`tandem-genotypes` can handle custom-made repeat annotation files in BED-like format. We made an annotation file with 31 repeat expansion disease loci, including BAFME, and analyzed these 31 repeats with our BAFME data. No large pathological expansions other than BAFME were predicted (Figure 7). We also analyzed these 31 repeats with each of the nanopore and PacBio datasets for NA12878: no obvious pathological expansions were predicted and peaks are around zero in most cases (Supplemental Figure 3, 4). These results suggest that our method does not spuriously predict pathological repeat expansions, although there may be some difficulties detecting small disease-causing expansions (e.g. +2 alanine expansion in *PABPN1* causes disease) due to deviations toward copy-number increase in PacBio sequences. We believe this will be solved when sequencing quality improves.

Prioritization of copy number changes

We also tested if it is possible to prioritize the detected copy number changes. The BAFME repeat expansion was ranked 13th out of 0.7 million

tandem repeat regions in rmsk.txt (Supplemental Figure 5). Repeat expansions in coding regions can cause disease with less than 100 extra copies, due to the high impact on proteins even from relatively small expansions. So these expansions may be difficult to prioritize. To test this, we combined `tandem-genotypes` output for the whole genome (NA12878 rel3) with outputs for the plasmid-rel3 chimeric reads with coding-region expansions (*ATN1*, *HTT*, *ATXN2*, *ATXN3*, *CACNA1A*, *ATXN7* and *AR*). All 7 chimeric expansions were ranked in the top 34 out of 0.7 million repeat regions (Supplemental Figure 6).

Comparing tandem repeat copy number change distribution of MinION, PromethION and Pacbio RSII sequencing data

We next examined the genome-wide repeat copy number changes in the NA12878 human genome sequenced by both PacBio RSII (SRR3197748) and Oxford Nanopore Technology's MinION (rel3). There was marked discordance between MinION and Pacbio when the repeat unit size was one or two (Figure 8a, Supplemental Figure 7). This is probably because MinION tends

to make small deletion errors and PacBio small insertion errors, which are hard to distinguish from copy number changes of these tiny repeat units. Note that a repeat unit size of one means homopolymers (such as AAAAAAAAAA). The triplet-repeat distribution showed a slight difference between MinION and PacBio (Figure 8a). However, where the repeat unit is longer than 3, MinION and PacBio had similar distributions of copy number changes (Supplemental Figure 7), so both sequencing platforms work on these tandem-repeats. We also verified that the GGGGCC strand bias, which we observed in the plasmids, is also seen in the rel3 dataset. The distribution of GGGGCC copy number change showed a slight difference between forward and reverse strands (Supplemental Figure 1b).

We examined the distribution of copy number change for all kinds of di-nucleotide and triplet repeat. There are four possible types of di-nucleotide repeat (AG, AT, CG and AC) and ten kinds of triplet repeat (TAA, GTC, AAC, GAT, CTT, CTG, GTA, CGG, CCT and CAC). MinION sequences (rel3) showed obvious systematic strand biases for AC, AG, CCT and CTT (Figure 8b,d,

Supplemental Figure 8-10). Note that we do not expect any strand bias for CG and AT because they are palindromic.

The MinION data we tested (rel3) was published in 2017. Nanopore base-callers and chemistries have been greatly improved recently. We tested a recent nanopore MinION dataset analyzed by MinKNOW1.11.5, which uses the Albacore 2.0 base-caller. The strand bias for AC, AG, CCT and CTT was greatly improved (Supplemental Figure 11). We also tested a recently published human genome dataset sequenced by ONT's new high throughput sequencer PromethION. We also found that strand biases for AC, AG, CTT and CCT are greatly improved in PromethION reads (Figure 8b,d, Supplemental Figures 12, 13).

Computation time and repeat-masking

The slowest computational step was aligning the reads to the genome (`lastal`). For some datasets, we made it much faster by “masking” repeats (both interspersed and tandem) with `WindowMasker`. Here, “masking” means

that the repeats (indicated by lowercase letters) are excluded from the similarity-search steps of the alignment algorithm, but are included when making the final alignments: the hope is to find the same alignments faster.

In practice, this masking is often harmless, but sometimes harmful. It did not prevent us from detecting the BAFME expansion, or expansions at 10 other disease loci in chimeric human/plasmid reads. On the other hand, it prevented detection of the SCA10 expansions (result not shown). This is because one flank of the SCA10 tandem repeat consists of transposable elements and is almost completely masked. Note this is an older dataset with somewhat short reads (Table 2): the problem would be solved by longer reads that extend beyond the masked region.

When we do not mask, the total run time for our analysis is competitive with those of RepeatHMM and PacmonSTR (Supplemental Table 3). (Note the last-train run time does not increase much for larger datasets, because it uses a fixed-size sample of the data.) When we do mask, the computation is much

faster (Supplemental Table 4), and usually the results do not change significantly (Supplemental Figure 14).

Discussion

We have presented several lines of evidence that we can robustly detect pathological expansions of tandem repeats. We successfully detected them in: constructed plasmids, semi-artificial plasmid/human sequences, and real human sequences from patients with SCA10 and BAFME. We also did *not* detect unexpected (false-positive) large known-pathological expansions in three whole-genome datasets: PacBio reads from a BAFME patient, and PacBio and nanopore reads from NA12878. Importantly, we can also rank copy-number changes by priority, such that pathological expansions are ranked near the top out of ~0.7 million tandem repeats in the genome.

Our method is not specific to tandem expansions, but detects any kind of expansion of a tandem repeat. For example, we detected an expansion due to insertion of an Alu SINE within a tandem repeat (Figure 5a). We also detected

an expansion that contained non-repeat sequence, which turned out to be a deletion in the reference genome (Figure 5b). Such non-tandem expansions may impact genomic function and health, so we believe it is useful to detect them too during first-round genome-wide screening.

If a repeat expansion is actually the ancestral state, with the reference genome having a contraction or deletion (e.g. Figure 5b), then it is plausible that the expansion is less likely to be pathological. Thus, our prioritization of copy-number changes could perhaps be improved by comparing the changes to ape genomes. An ancestral reference human genome would be ideal[14]. A similar idea is to de-prioritize expansions commonly present in healthy humans: this will become more powerful as tandem repeat data accumulates.

We have also pointed out some interesting difficulties with analyzing tandem repeat sequences. Some DNA reads do not align to the repetitive region of the reference genome (e.g. Figure 6b), and systematic sequencing errors may turn a tandem repeat into a different tandem repeat. The analysis becomes harder when the reference sequence next to an annotated tandem repeat

resembles the sequence in the repeat (e.g. Figure 6c). Some (inexact) tandem repeats do not have unambiguous boundaries, and different annotations (e.g. RepeatMasker versus Tandem Repeats Finder[25]) sometimes disagree on the boundaries. In some cases, there may be no unambiguous distinction between expansion of a tandem repeat and sequence insertion near the repeat.

Systematic sequencing errors can have different effects on the two strands of tandemly-repeated DNA, causing the predicted copy number changes to have a bimodal distribution (e.g. Figure 1i). So it is important to indicate which predictions come from which strands, in order to not misinterpret this as two alleles. We report length and strand biases of several long-read sequencers for every possible type of di- and tri-nucleotide repeat: these biases are prominent for specific repeats (e.g. CTT and CCT in older MinION data), and the worst biases are greatly improved in more recent sequencing systems.

If sequencing accuracy continues to improve, tandem repeat analysis will obviously benefit. The alignment will automatically become faster, due to

lower tolerance of gaps and substitutions. Copy number will be predictable more accurately and with lower coverage.

This study demonstrates a practical and robust way to identify changes in tandem repeats that may have biologically impactful consequences. Although there are still limitations due to the developing sequencing technologies and cost to immediately apply this approach in clinical sequencing, we clearly show that there is hope that long read sequencing is useful to identify overlooked changes in the genome, and may give an answer to the large numbers of patients with genetic diseases whose causes and mechanisms have remained unsolved for many years.

Funding

This work was supported by AMED under grant numbers, JP18ek0109280, JP18dm0107090 and JP18ek0109301; JSPS KAKENHI Grant Numbers, JP17H01539, JP17K16132 and JP16K09683; Takeda Science Foundation;

Kawano Masanori Memorial Public Interest Incorporated Foundation for Promotion of Pediatrics; and Dementia Drug Resource Development Center Project (S1511016).

Acknowledgements

MCF thanks Masahiro Onoguchi for pointing out that strand bias must be discriminated from heterozygosity. SM thanks to Qian Liu for suggesting parameters for SCA10 data analyses using RepeatHMM. YK thanks Jun-ichi Satoh and Mika Takitani for plasmid construction. Sanger sequencing was performed by the Support Center for Medical Research and Education, Tokai University.

Author contributions

SM and MCF contributed to the conception of the work, acquisition, analysis and interpretation of the data T.M, S.M, T.T, H.A, Y.O, Y.K, H.M and N.M contributed to obtaining and making the materials and acquisition and analysis of data.

Competing interests

None of the authors have competing interests.

Figure legends

Figure 1

Distribution of predicted change in repeat copy number, for nanopore reads from each of ten plasmids. Red arrows: projected copy number change. Forward (red) and reverse strand reads (blue) are shown separately. y-axis: read count, x-axis: change in copy number relative to the reference plasmid. Reference copy numbers in each plasmid are in Supplemental Table 1. Black arrows: reads in these peaks may actually have shortened repeats.

Figure 2

Distribution of predicted change in repeat copy number, for random samples of plasmid nanopore reads. Coverages 50, 30 and 15 were tested. (a) CAG

repeats. (b) CAA repeats. (c) GGGGCC repeats. y-axis: read count, x-axis: change in copy number relative to the reference plasmid.

Figure 3

Distribution of predicted change in repeat copy number, for nanopore reads of human DNA with inserted repeats. Reads covering each of ten disease-associated repeat loci were selected, and the repeat region in each read was replaced by: the repeat region of a plasmid nanopore read (a-j top panels), or exact repeats (a-j bottom panels). y-axis: read count, x-axis: change in copy number relative to the reference human genome. Forward (red) and reverse strand reads (blue) are shown separately.

Figure 4

Distribution of predicted change in repeat copy number, for PacBio (RSII) reads of cloned SCA10 loci from 3 patients. (a) `tandem-genotypes`. Forward (red) and reverse strand reads (blue) are shown separately. (b) RepeatHMM with

straightforward parameters. (c) RepeatHMM with non-obvious parameters suggested by its authors. y-axis: read count, x-axis: change in copy number relative to the reference human genome.

Figure 5

PCR results and Sanger sequencing of two tandem-repeat loci in human genome NA12878, with expansions relative to the reference human genome (hg38). The histograms show read counts (y-axis) for predicted copy number changes (x-axis), with nanopore (rel3) in blue and PacBio (SRR3197748) in red (a) Expansion of an inexact TATAT repeat in an intron of *PCDH15*: actually insertion of an AluYb8 SINE. (b) Expansion of an intergenic GT repeat: actually deletion in the reference human genome. The bands marked by * were sequenced and proved to be non-target amplification.

Figure 6

Alignments of DNA reads (vertical) to the reference human genome (horizontal). Diagonal lines indicate alignments, of same strands (red) and opposite strands (blue). The vertical stripes indicate repeat annotations in the reference genome: tandem repeats (purple) and transposable elements (pink). (a) Six reads from a BAFME patient that cover the disease-causing *SAMD12* AAAAT repeat locus. (b) Close-ups of three reads with ~5k expansions. (c) Two examples of chimeric human reads (rel3) with expanded CAG repeats at the *ATXN7* disease locus.

Figure 7

Changes in disease-associated repeats of a BAFME patient. The *SAMD12* locus (red border) shows clear expansion of around 900 copies, and is prioritized 1st among 31 disease loci. The other loci have no obvious pathogenic expansions. Forward (red) and reverse strand reads (blue) are shown separately. These histograms were made by `tandem-genotypes-plot`.

Figure 8

(a) Genome-wide distribution of predicted change in repeat copy number, for nanopore MinION (rel3) and PacBio (SRR3197748) reads from the same human (NA12878). Nanopore tends to have negative and PacBio positive predicted changes, especially for short repeat units. Read number = 10,000 (randomly sampled). Nanopore reads are shown in blue and PacBio in red. (b-d) Genome-wide distribution of predicted change in repeat copy number for nanopore MinION (rel3) and PacBio (SRR3197748) reads from the same human (NA12878), and nanopore PromethION (ERR2585112-5) from a different individual (NA19240). (b) Distributions for AG dinucleotide repeats. (c) Distributions for GAT. (d) Distributions for CTT. CTT shows the most prominent strand bias in nanopore rel3 reads among all types of triplet repeat (all types are in Supplemental Figures 8-13). PromethION shows less strand bias compared to rel3. y-axis: read count, x-axis: change in copy number relative to the reference human genome.

Reference

1. Tang H, Kirkness EF, Lippert C, et al. Profiling of Short-Tandem-Repeat Disease Alleles in 12,632 Human Whole Genomes. Am J Hum Genet 2017;101:700-15.

2. La Spada AR, Roling DB, Harding AE, et al. Meiotic stability and genotype-phenotype correlation of the trinucleotide repeat in X-linked spinal and bulbar muscular atrophy. Nat Genet 1992;2:301-4.

3. A novel gene containing a trinucleotide repeat that is expanded and unstable on Huntington's disease chromosomes. The Huntington's Disease Collaborative Research Group. Cell 1993;72:971-83.

4. Brook JD, McCurrach ME, Harley HG, et al. Molecular basis of myotonic dystrophy: expansion of a trinucleotide (CTG) repeat at the 3' end of a transcript encoding a protein kinase family member. Cell 1992;68:799-808.

5. Kremer EJ, Pritchard M, Lynch M, et al. Mapping of DNA instability at the fragile X to a trinucleotide repeat sequence p(CCG)n. Science 1991;252:1711-4.

6. Lemmers RJ, van der Vliet PJ, Klooster R, et al. A unifying genetic model for facioscapulohumeral muscular dystrophy. Science 2010;329:1650-3.

7. Brais B, Bouchard JP, Xie YG, et al. Short GCG expansions in the PABP2 gene cause oculopharyngeal muscular dystrophy. Nat Genet 1998;18:164-7.

8. Musova Z, Mazanec R, Krepelova A, et al. Highly unstable sequence interruptions of the CTG repeat in the myotonic dystrophy gene. Am J Med Genet A 2009;149A:1365-74.

9. McFarland KN, Liu J, Landrian I, et al. SMRT Sequencing of Long Tandem Nucleotide Repeats in SCA10 Reveals Unique Insight of Repeat Expansion Structure. PLoS One 2015;10:e0135906.

10. Ishiura H, Doi K, Mitsui J, et al. Expansions of intronic TTTCA and TTTTA repeats in benign adult familial myoclonic epilepsy. Nat Genet 2018;50:581-90.

11. Nishikawa A, Mitsuhashi S, Miyata N, Nishino I. Targeted massively parallel sequencing and histological assessment of skeletal muscles for the

molecular diagnosis of inherited muscle disorders. J Med Genet 2017;54:104-10.

12. Ummat A, Bashir A. Resolving complex tandem repeats with long reads. Bioinformatics 2014;30:3491-8.

13. Liu Q, Zhang P, Wang D, Gu W, Wang K. Interrogating the "unsequenceable" genomic trinucleotide repeat disorders by long-read sequencing. Genome Med 2017;9:65.

14. Frith MC, Khan S. A survey of localized sequence rearrangements in human DNA. Nucleic Acids Res 2018;46:1661-73.

15. Hamada M, Ono Y, Asai K, Frith MC. Training alignment parameters for arbitrary sequencers with LAST-TRAIN. Bioinformatics 2017;33:926-8.

16. Frith MC. A new repeat-masking method enables specific detection of homologous sequences. Nucleic Acids Res 2011;39:e23.

17. Frith MC. Gentle masking of low-complexity sequences improves homology search. PLoS One 2011;6:e28819.

18. Jain M, Koren S, Miga KH, et al. Nanopore sequencing and assembly of a human genome with ultra-long reads. Nat Biotechnol 2018;36:338-45.

19. Oma Y, Kino Y, Sasagawa N, Ishiura S. Intracellular localization of homopolymeric amino acid-containing proteins expressed in mammalian cells. J Biol Chem 2004;279:21217-22.

20. Kino Y, Washizu C, Kurosawa M, et al. Nuclear localization of MBNL1: splicing-mediated autoregulation and repression of repeat-derived aberrant proteins. Hum Mol Genet 2015;24:740-56.

21. Oma Y, Kino Y, Toriumi K, Sasagawa N, Ishiura S. Interactions between homopolymeric amino acids (HPAAs). Protein Sci 2007;16:2195-204.

22. O'Leary NA, Wright MW, Brister JR, et al. Reference sequence (RefSeq) database at NCBI: current status, taxonomic expansion, and functional annotation. Nucleic Acids Res 2016;44:D733-45.

23. Morgulis A, Gertz EM, Schaffer AA, Agarwala R. WindowMasker: window-based masker for sequenced genomes. Bioinformatics 2006;22:134-41.

24. Nakamura K, Oshima T, Morimoto T, et al. Sequence-specific error profile of Illumina sequencers. Nucleic Acids Res 2011;39:e90.

25. Benson G. Tandem repeats finder: a program to analyze DNA sequences. Nucleic Acids Res 1999;27:573-80.

26. Edgar RC. MUSCLE: multiple sequence alignment with high accuracy and high throughput. Nucleic Acids Res 2004;32:1792-7.

chr	start	end	repeat	gene	region	repeat number in reference	inserted repeat 1	inserted repeat 2	expected change 1	expected change 2	read number 1	read number 2	tandem-genotypes detected	total mapped reads
chr3	63,912,686	63,912,715	CAG	*ATXN7*	coding	10	6	30	-4	20	24	24	28	30
chr3	129,172,577	129,172,656	CCTG	*CNBP*	intron	21	raw-data	45	NA	24	18	17	31	33
chr4	3,074,877	3,074,933	CAG	*HTT*	coding	21	6	70	-15	49	21	20	31	38
chr5	146,878,729	146,878,758	CAG	*PPP2R2B*	intron	10	6	70	-4	60	11	10	21	21
chr9	27,573,529	27,573,546	GGGGCC	*C9orf72*	intron	3	21	52	18	49	14	14	23	26
chr12	6,936,729	6,936,773	CAG	*ATN1*	coding	15	18	70	3	55	18	20	36	38
chr12	111,598,951	111,599,019	CAG	*ATXN2*	coding	23	30	70	7	47	20	20	34	36
chr14	92,071,011	92,071,034	CAG	*ATXN3*	coding	10	6	130	-4	120	15	15	30	30
chr19	13,207,859	13,207,897	CAG	*CACNA1A*	coding	13	6	30	-7	17	18	17	31	34
chrX	67,545,318	67,545,383	CAG	*AR*	coding	23	18	70	-5	47	21	20	18	22

Table 1 Chimera reads

name	type	Sequencer	individual ID	Accession number	bases	reads	average length	median
rel3	human genome	MinION	NA12878	*	91,240,120,433	14,183,584	6,432.8	4617.0
SRR3197748	human genome	RSII	NA12878	SRR3197748	176,931,641,323	40,820,704	4,334.4	3053.0
ERR2585112-5	human genome	PromethION	NA19240	ERR2585112-5	185,056,318,464	13,134,890	14,088.9	12551.0
BAFME	human genome	Sequel	(private)	(private)	44,835,599,221	6,174,384	7,261.6	6324.0
CAA-15	plasmid	MinION	-	DRR140497	3,312,623	726	4,562.8	4689.5
CAA-109	plasmid	MinION	-	DRR140498	2,861,064	597	4,792.4	4962.0
GGGGCC-52	plasmid	MinION	-	DRR140499	228,298,911	50,884	4,486.7	4439.0
GGGGCC-21	plasmid	MinION	-	DRR140500	305,112,100	71,016	4,296.4	4600.0
CAG-6	plasmid	MinION	-	DRR140501	170,853,052	59,808	2,856.7	2935.0
CAG-18	plasmid	MinION	-	DRR140502	177,739,795	31,644	5,616.9	5887.0
CAG-30	plasmid	MinION	-	DRR140503	420,957,360	142,000	2,964.5	2999.0
CAG-30-DraIII	plasmid	MinION	-	DRR140504	104,545,063	33,551	3,116.0	3026.0
CAG-70	plasmid	MinION	-	DRR140505	64,609,201	18,232	3,543.7	3091.5
CAG-130	plasmid	MinION	-	DRR140506	10,215,540	2,135	4,784.8	5002.0
CCTG-45	plasmid	MinION	-	DRR140507	3,675,433	875	4,200.5	4605.0
SCA10-subjectA	plasmid	RSII	-	SRR2080459	92,385,186	81,623	1,131.9	642.0
SCA10-subjectB	plasmid	RSII	-	SRR2081063	303,000,762	81,740	3,706.9	2605.0
SCA10-subjectC-1	plasmid	RSII	-	SRR2082412	157,578,422	81,741	1,927.8	893.0
SCA10-subjectC-2	plasmid	RSII	-	SRR2082428	611,539,771	163,476	3,740.9	1834.0
AR-chimera	rel3-plasmid	MinION	-	-	869,853	41	21,215.9	13224.0
HTT-chimera	rel3-plasmid	MinION	-	-	518,235	40	12,955.9	7462.5
CACNA1A-chimera	rel3-plasmid	MinION	-	-	387,962	35	11,084.6	9411.0
C9orf72-chimera	rel3-plasmid	MinION	-	-	330,265	26	12,702.5	9054.5
ATXN2-chimera	rel3-plasmid	MinION	-	-	627,855	40	15,696.4	8155.0
ATXN3-chimera	rel3-plasmid	MinION	-	-	465,481	30	15,516.0	14225.0
ATXN7-chimera	rel3-plasmid	MinION	-	-	795,136	48	16,565.3	9921.5
ATN1-chimera	rel3-plasmid	MinION	-	-	374,363	38	9,851.7	8863.0
PPP2R2B-chimera	rel3-plasmid	MinION	-	-	334,450	21	15,926.2	8899.0
CNBP-chimera	rel3-plasmid	MinION	-	-	361,861	34	10,643.0	9349.0

Table 2. Dataset information
*Downloaded from https://github.com/nanopore-wgs-consortium/NA12878

Figure 1

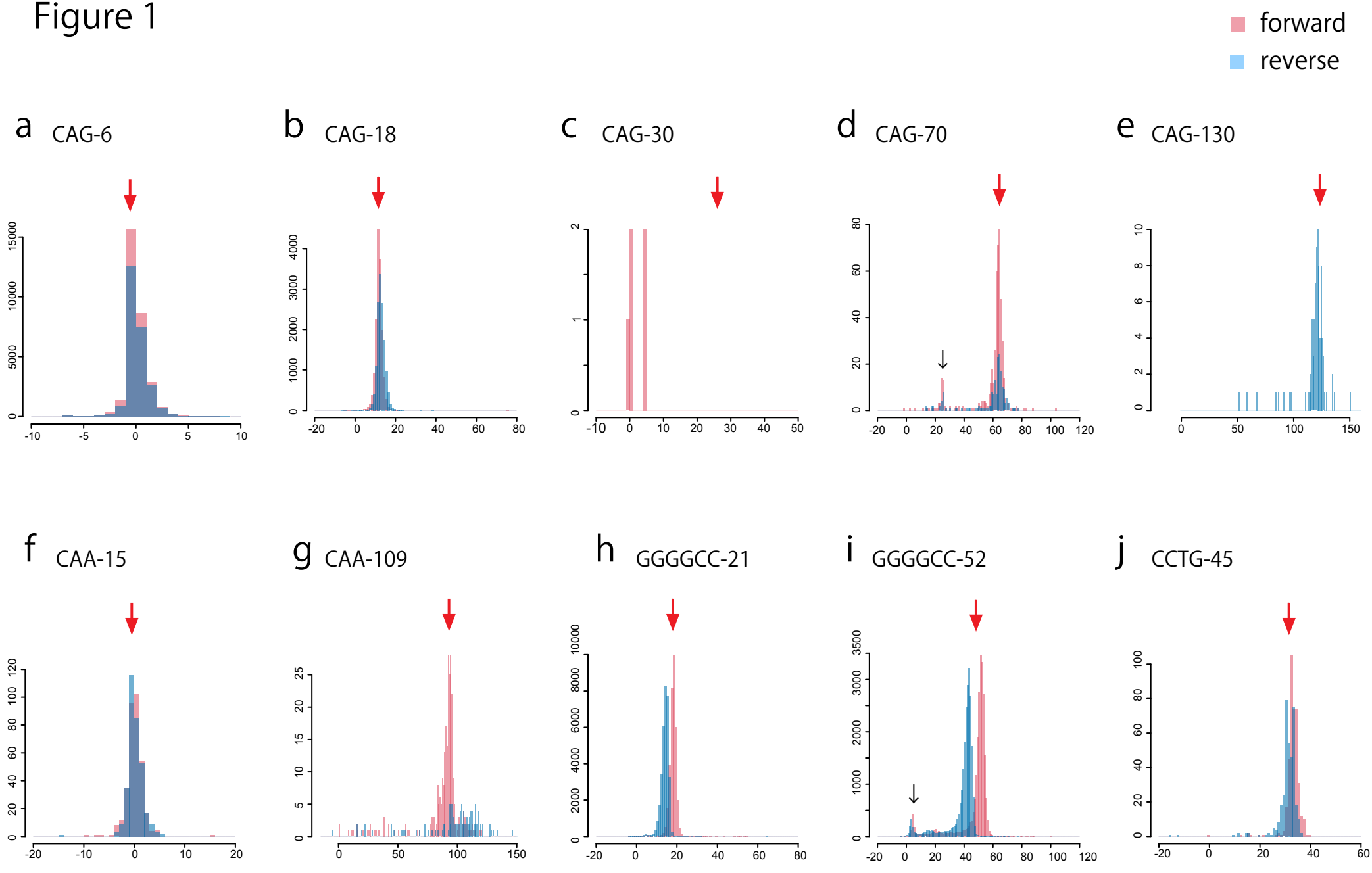
forward
reverse
a CAG-6
b CAG-18
c CAG-30
d CAG-70
e CAG-130
f CAA-15
g CAA-109
h GGGGCC-21
i GGGGCC-52
j CCTG-45

Figure 2

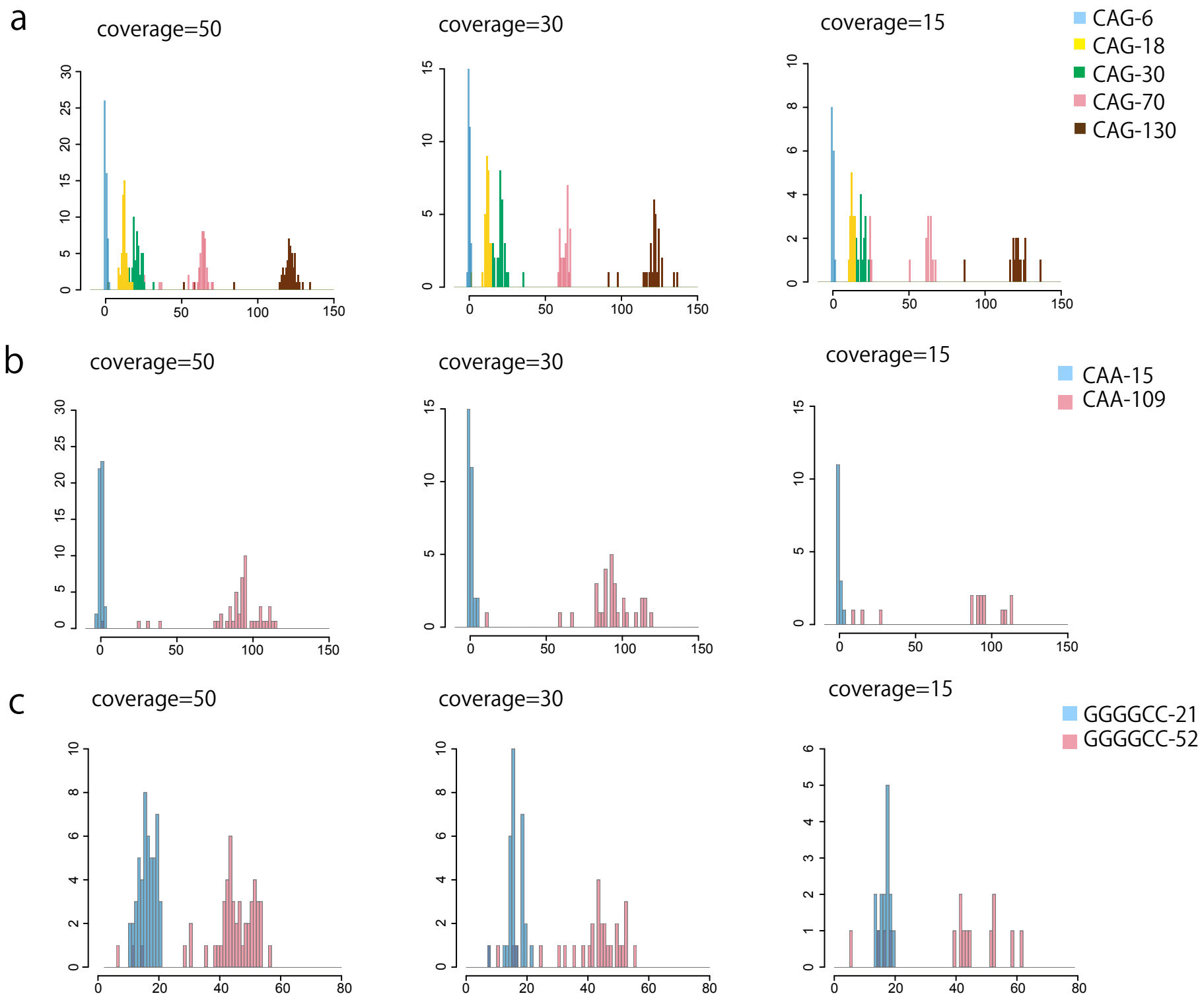
a
coverage=50
coverage=30
coverage=15
CAG-6
CAG-18
CAG-30
CAG-70
CAG-130
b
coverage=50
coverage=30
coverage=15
CAA-15
CAA-109
c
coverage=50
coverage=30
coverage=15
GGGGCC-21
GGGGCC-52

Figure 3

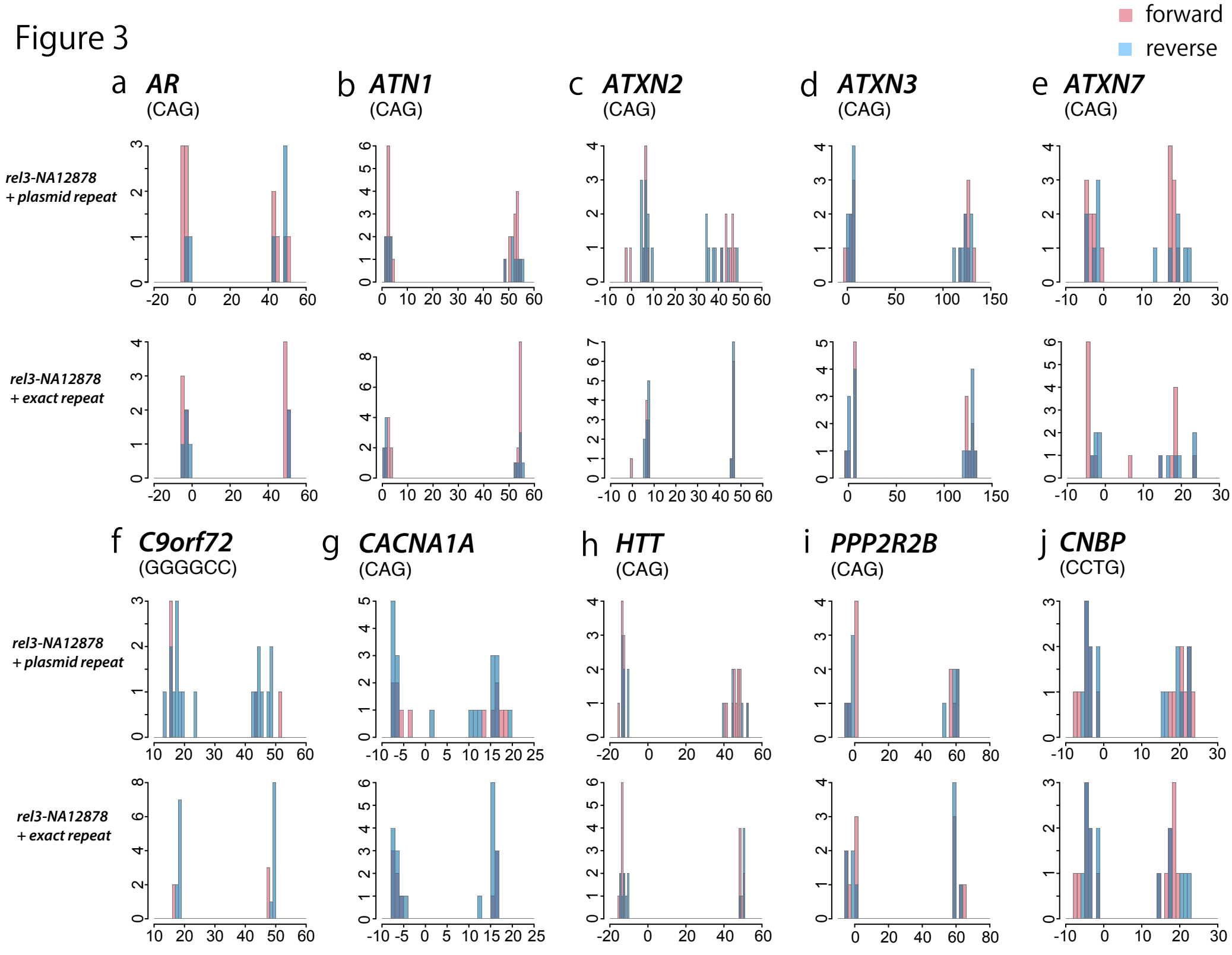
forward
reverse
a AR (CAG)
b ATN1 (CAG)
c ATXN2 (CAG)
d ATXN3 (CAG)
e ATXN7 (CAG)
rel3-NA12878 + plasmid repeat
rel3-NA12878 + exact repeat
f C9orf72 (GGGGCC)
g CACNA1A (CAG)
h HTT (CAG)
i PPP2R2B (CAG)
j CNBP (CCTG)
rel3-NA12878 + plasmid repeat
rel3-NA12878 + exact repeat

Figure 4

a

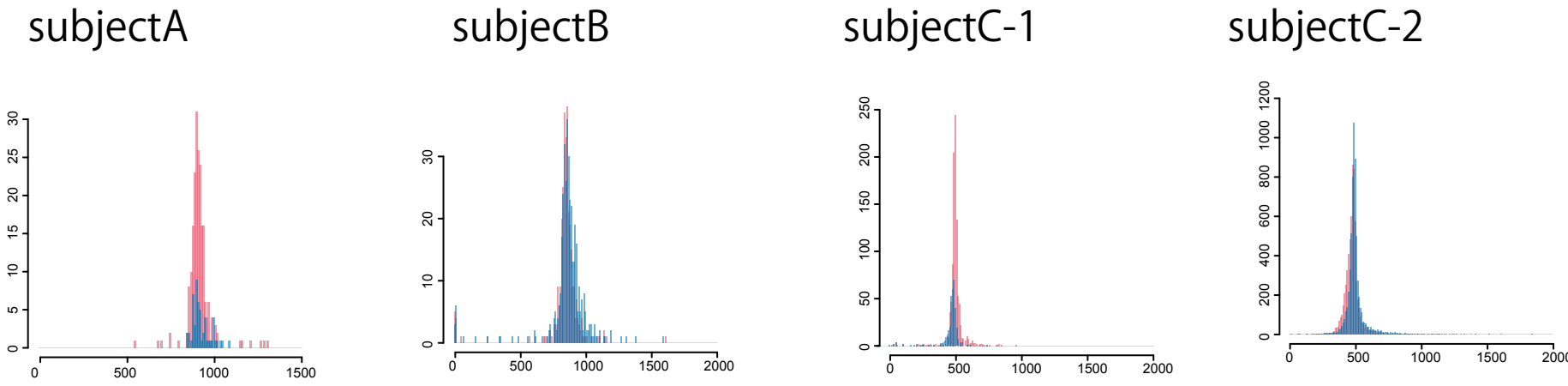
subjectA
subjectB
subjectC-1
subjectC-2

b

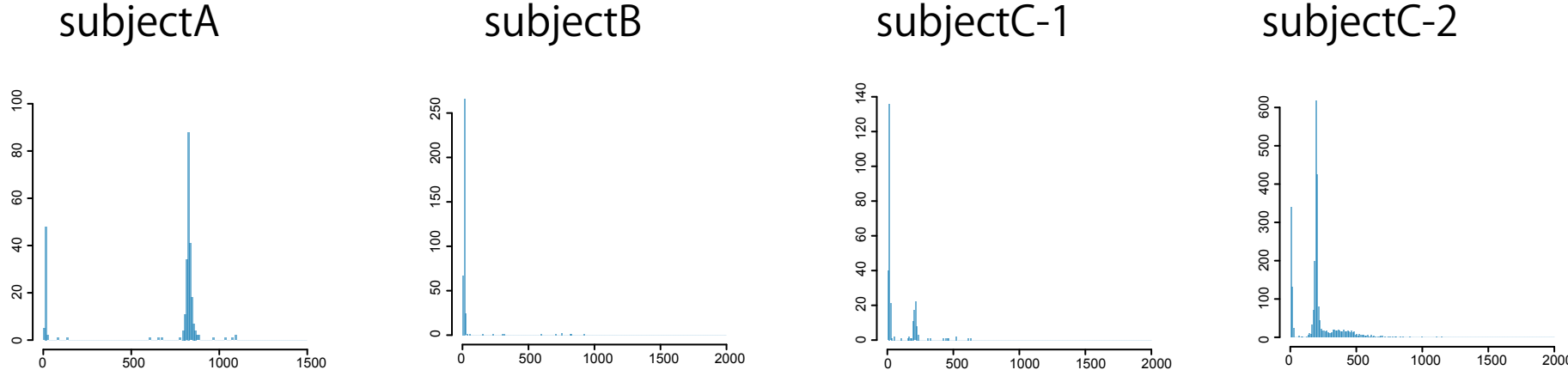
subjectA
subjectB
subjectC-1
subjectC-2

c

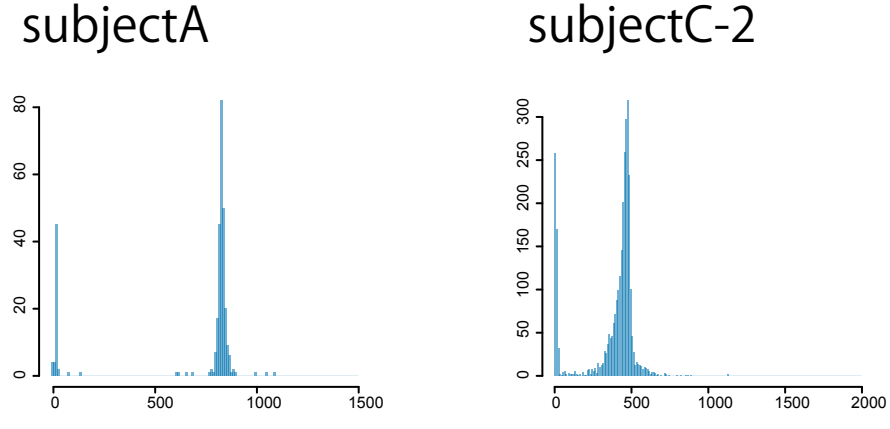
subjectA
subjectC-2

Figure 5

a

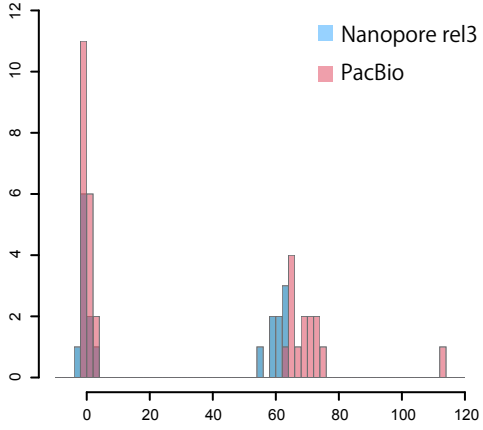

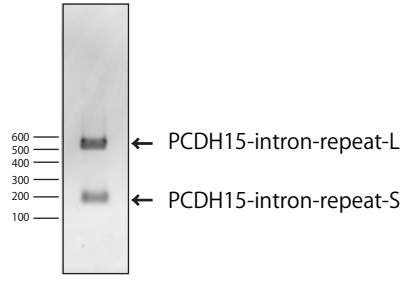

b

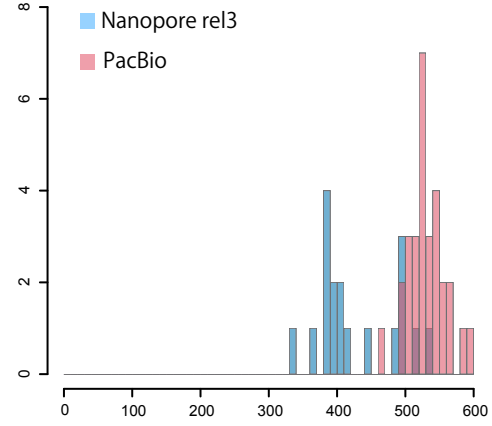

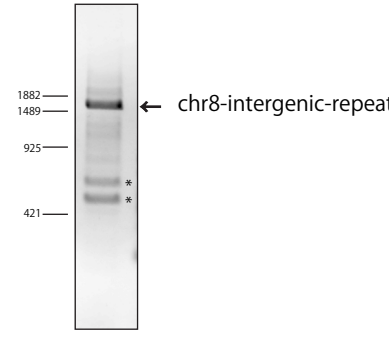

PCDH15-intron-repeat-L

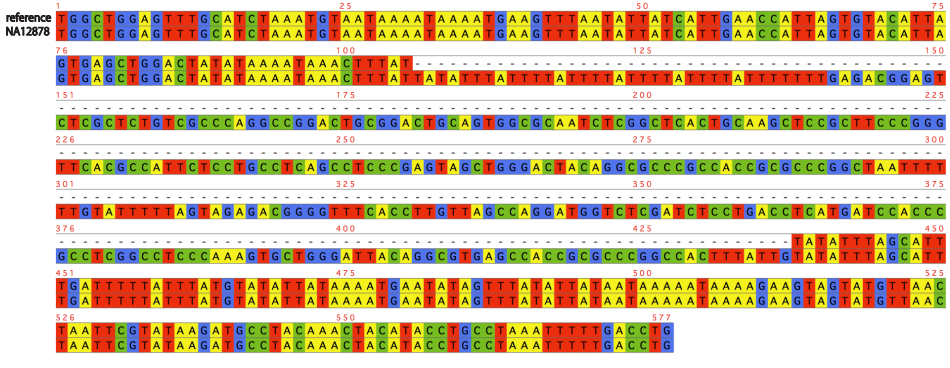

PCDH15-intron-repeat-S

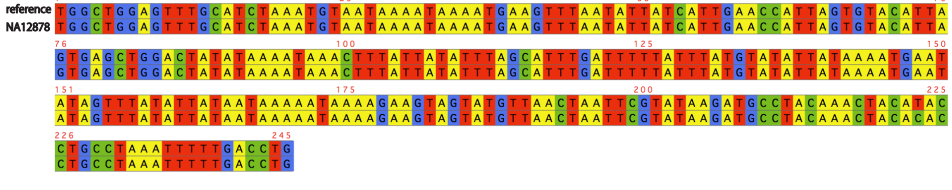

chr8-intergenic-repeat

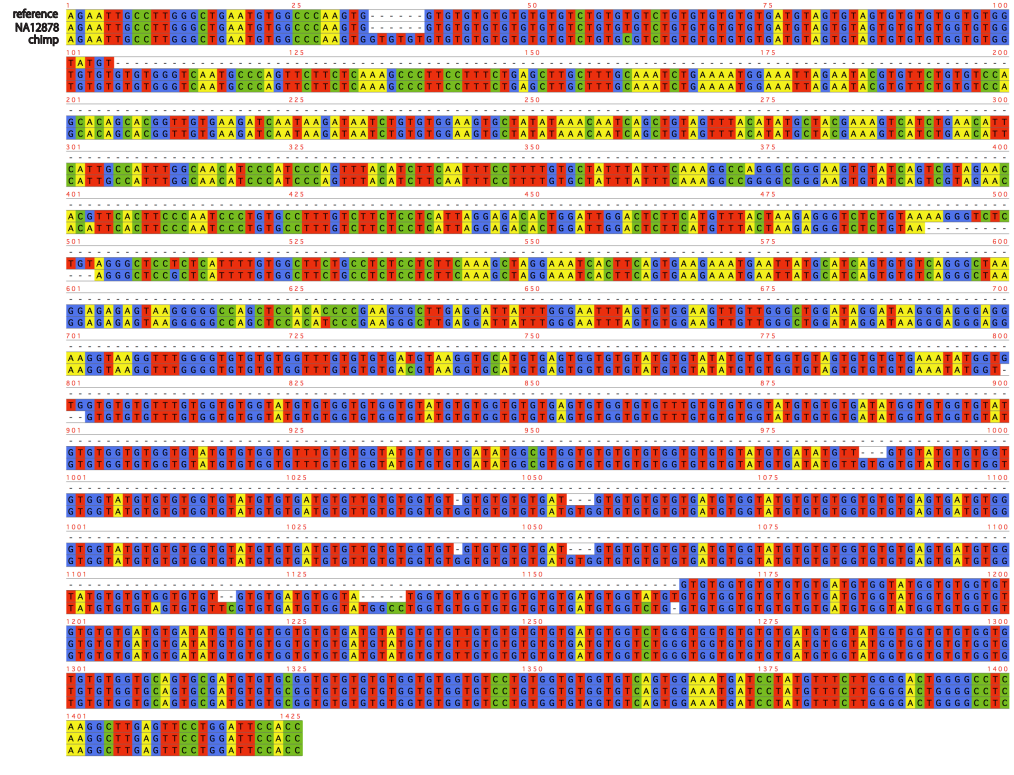

Figure 6

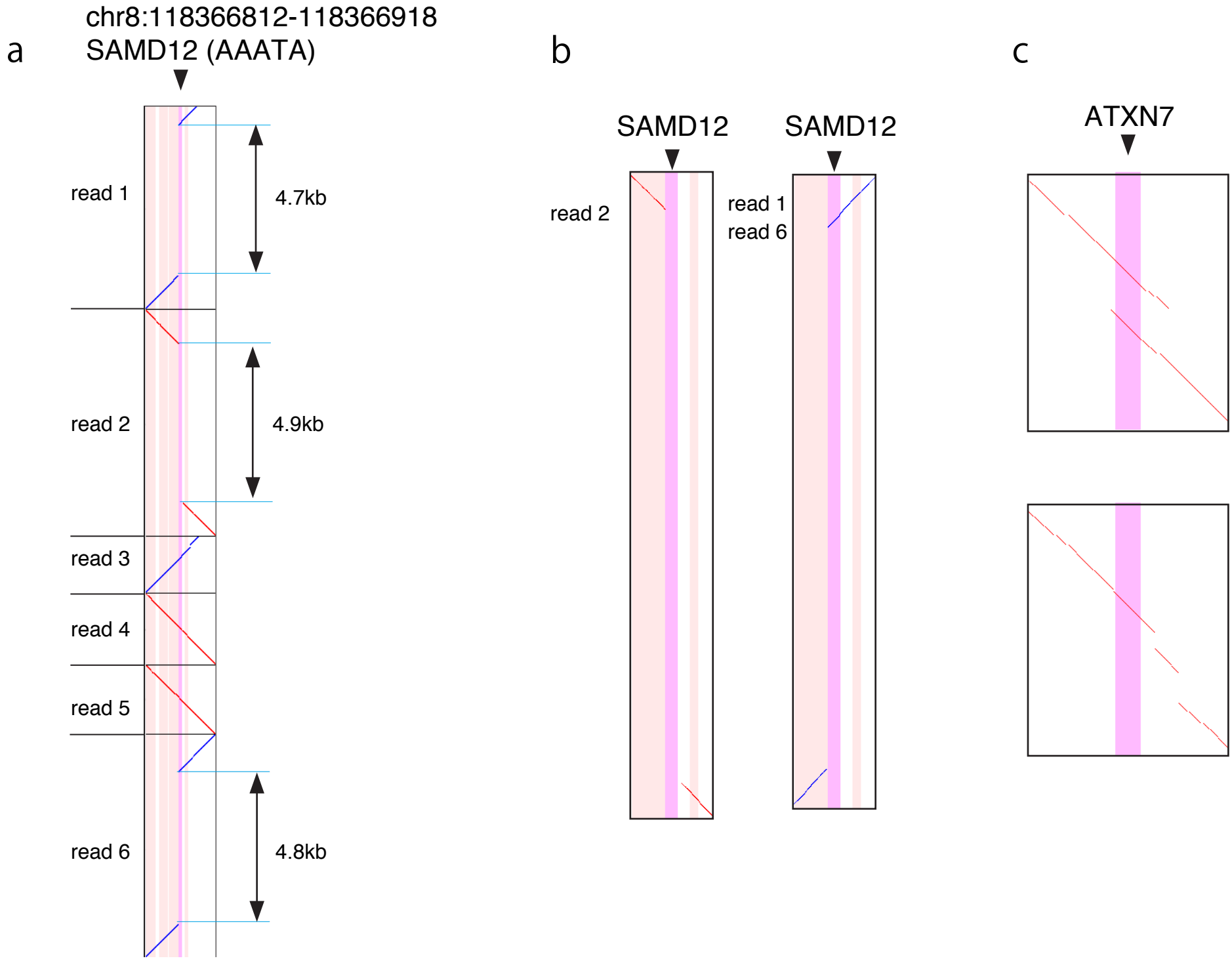
a
chr8:118366812-118366918
SAMD12 (AAATA)
read 1
read 2
read 3
read 4
read 5
read 6
4.7kb
4.9kb
4.8kb
b
SAMD12
read 2
SAMD12
read 1
read 6
c
ATXN7

Figure 7

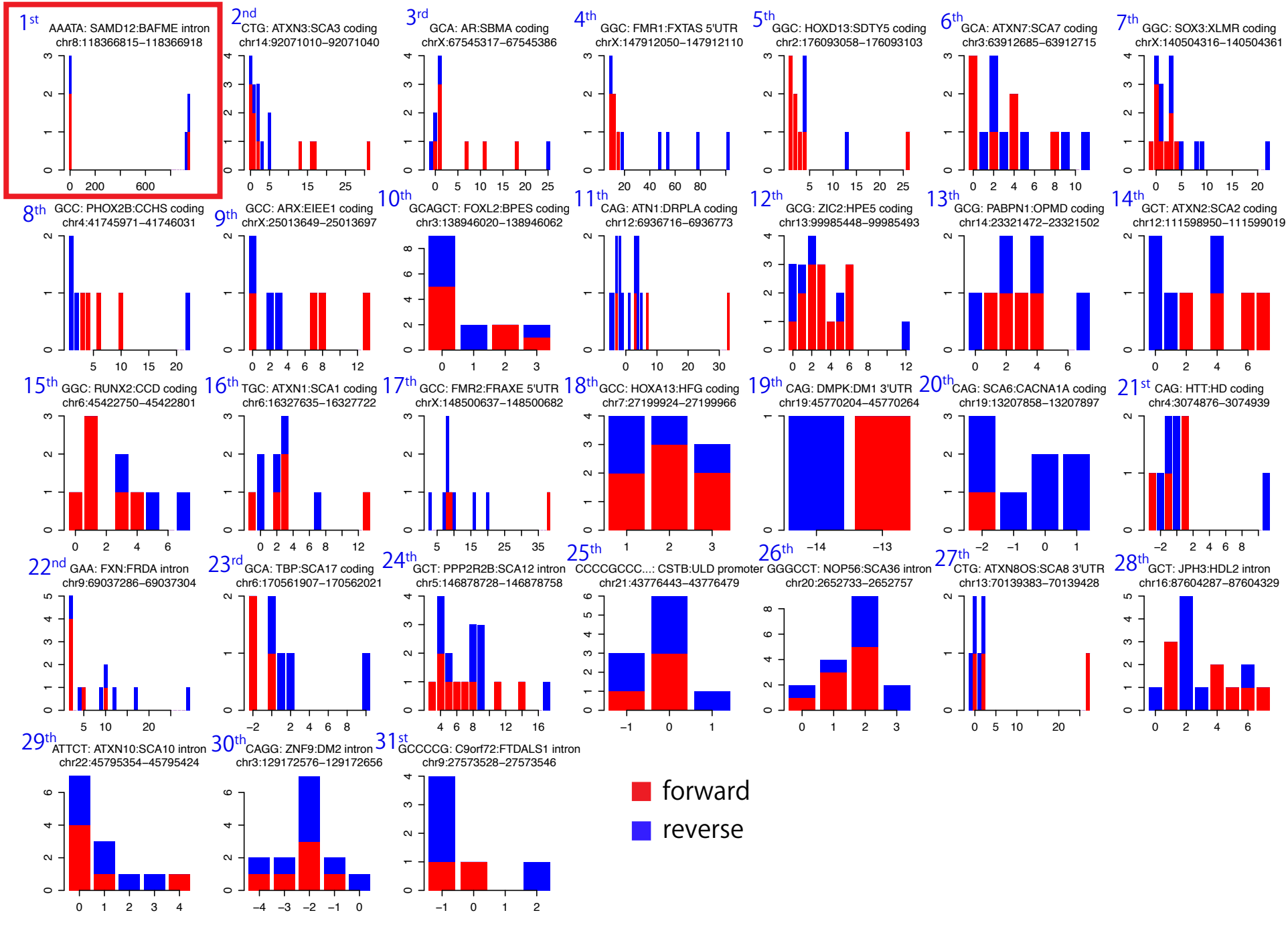
1st AAATA: SAMD12:BAFME intron chr8:118366815–118366918
2nd CTG: ATXN3:SCA3 coding chr14:92071010–92071040
3rd GCA: AR:SBMA coding chrX:67545317–67545386
4th GGC: FMR1:FXTAS 5'UTR chrX:147912050–147912110
5th GGC: HOXD13:SDTY5 coding chr2:176093058–176093103
6th GCA: ATXN7:SCA7 coding chr3:63912685–63912715
7th GGC: SOX3:XLMR coding chrX:140504316–140504361
8th GCC: PHOX2B:CCHS coding chr4:41745971–41746031
9th GCC: ARX:EIEE1 coding chrX:25013649–25013697
10th GCAGCT: FOXL2:BPES coding chr3:138946020–138946062
11th CAG: ATN1:DRPLA coding chr12:6936716–6936773
12th GCG: ZIC2:HPE5 coding chr13:99985448–99985493
13th GCG: PABPN1:OPMD coding chr14:23321472–23321502
14th GCT: ATXN2:SCA2 coding chr12:111598950–111599019
15th GGC: RUNX2:CCD coding chr6:45422750–45422801
16th TGC: ATXN1:SCA1 coding chr6:16327635–16327722
17th GCC: FMR2:FRAXE 5'UTR chrX:148500637–148500682
18th GCC: HOXA13:HFG coding chr7:27199924–27199966
19th CAG: DMPK:DM1 3'UTR chr19:45770204–45770264
20th CAG: SCA6:CACNA1A coding chr19:13207858–13207897
21st CAG: HTT:HD coding chr4:3074876–3074939
22nd GAA: FXN:FRDA intron chr9:69037286–69037304
23rd GCA: TBP:SCA17 coding chr6:170561907–170562021
24th GCT: PPP2R2B:SCA12 intron chr5:146878728–146878758
25th CCCCGCCC...: CSTB:ULD promoter chr21:43776443–43776479
26th GGGCCT: NOP56:SCA36 intron chr20:2652733–2652757
27th CTG: ATXN8OS:SCA8 3'UTR chr13:70139383–70139428
28th GCT: JPH3:HDL2 intron chr16:87604287–87604329
29th ATTCT: ATXN10:SCA10 intron chr22:45795354–45795424
30th CAGG: ZNF9:DM2 intron chr3:129172576–129172656
31st GCCCCG: C9orf72:FTDALS1 intron chr9:27573528–27573546
forward
reverse

Figure 8

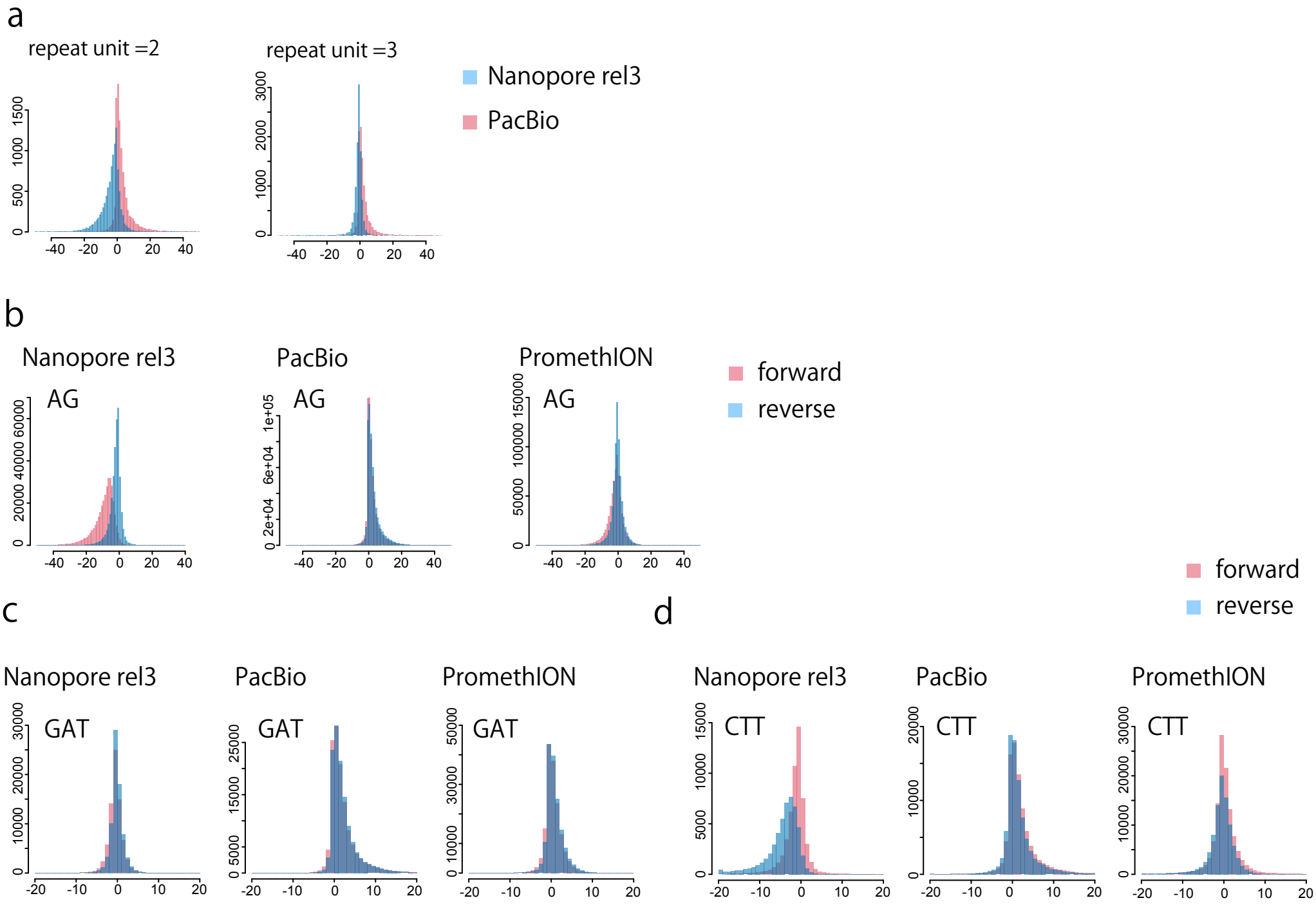
a
repeat unit =2
repeat unit =3
Nanopore rel3
PacBio
b
Nanopore rel3
PacBio
PromethION
AG
forward
reverse
c
d
Nanopore rel3
PacBio
PromethION
GAT
CTT
forward
reverse